biomolecules

MDPI

Article

4-Hydroxy-1α,25-Dihydroxyvitamin D3: Synthesis and Structure-Function Study

Carole Peluso-Iltis [1,2,3,4], Noé Pierrat [1,2,3,4], Daniela Rovito [1,2,3,4], Judit Osz [1,2,3,4], Daisuke Sawada [5], Atsushi Kittaka [6], Gilles Laverny [1,2,3,4] and Natacha Rochel [1,2,3,4,*]

[1] Institute of Genetics and Molecular and Cellular Biology (IGBMC), Illkirch, France
[2] CNRS UMR 7104, Illkirch, France
[3] Inserm U1258, Illkirch, France
[4] University of Strasbourg, Illkirch, France
[5] Graduate School of Medicine, Dentistry and Pharmaceutical Sciences, Okayama University, 1-1-1 Tsushimanaka, Kita-ku, Okayama-shi, Okayama, 700-8530 Japan
[6] Faculty of Pharmaceutical Sciences, Teikyo University, Tokyo, Japan
* Correspondence: rochel@igbmc.fr; Tel.: +33-369-48-52-93

Abstract: The active vitamin D metabolites, 25-hydroxyvitamin D3 (25D3) and 1,25-dihydroxyvitamin D3 (1,25D3), produced by successive hydroxylation steps, play key roles in several cellular processes. However, alternative metabolic pathways exist, and among them the 4-hydroxylation of $25D_3$ is a major one. This study aims to investigate the structure-activity relationships of 4-hydroxy derivatives of 1,25D3. Structural analysis indicates that $1,4\alpha,25(OH)_3D_3$ and $1,4\beta,25(OH)_3D_3$ maintain the anchoring hydrogen-bonds of $1,25D_3$ and form additional interactions, stabilizing the VDR active conformation. In addition, $1,4\alpha,25D_3$ and $1,4\beta,25D_3$ are as potent as 1,25D3 in regulating the expression of VDR target genes in rat intestinal epithelial cells and in mouse kidney. Moreover, these two 4-hydroxy derivatives promote hypercalcemia in mice at a dose similar to that of the parent compound.

Keywords: vitamin D metabolites; synthesis; calcemia; structure-function

1. Introduction

The biologically hormonal form of vitamin D, 1α,25-dihydroxyvitamin D3 ($1,25D_3$), regulates numerous biological processes comprising calcium metabolism, cell growth, differentiation, anti-proliferation, apoptosis and adaptive/innate immune responses [1-3]. These effects are mediated via binding of the hormone to its nuclear receptor, VDR (NR1I1) [4,5]. Classical pathways of $1,25D_3$ activation involve 25-hydroxylation by one of the 25-hydroxylase and 1α-hydroxylation by CYP27B1 [6]. General pathway associated to degradation of $1,25D_3$ involves side chain oxidation by CYP24A1 leading to catabolic excreted vitamin D metabolites including calcitroic acid, $1,25(OH)_2D_3$-26,23S-lactone, and (23S,25R),$25D_3$-(26,23)-lactone [7]. However, other metabolic and catabolic pathways are now recognized as being crucially important to vitamin D function and some metabolites have been shown to be biological active [8-9]. Among them, the $1\alpha,3epi,25D_3$, a metabolite modified at the A-ring, has been shown to retain significant biological activity compared to $1,25D_3$ [10] . In addition, A-ring natural metabolites modified at C4 were also reported. The $4,25D_2$ was initially identified from the serum of rats intoxicated with high concentrations of vitamin D2 [11]. Further *in vitro* and *in vivo* studies have characterized the occurrence of a C4 hydroxylation pathway that involves CYP3A4 enzyme [12,13]. Indeed, $4\alpha,25D_3$ and $4\beta,25D_3$ are CYP3A4-catalyzed metabolites of $25D_3$ (Figure 1A). Whereas $4\alpha,25D_3$ could only be detected in some studies, the levels of $4\beta,25D_3$, identified as an endogenous circulating metabolite in human plasma, are similar to those of $1,25D_3$ [12]. In

addition, significant accumulation of 4β,25D$_3$ was observed in the plasma of healthy subjects treated with rifampin, a Pregnane X Receptor (PXR) agonist that induces CYP3A4 [13]. Moreover, high levels of 4β,25D$_3$ were detected in patients exhibiting rickets and associated with CYP3A4 mutation [14]. However, 1,25D$_3$ is also a substrate for CYP3A4 leading to 1,23,25D$_3$ and inactivation[12,15].

Thus, 4-hydroxylation is a major pathway of 25D$_3$ metabolism. However, occurence of 4-hydroxylation of 1,25D$_3$ by CYP3A4 remains to be demonstrated and the biological significance of the 4-hydroxymetabolites remains elusive. The only available biological data concerned the synthetic 1,4α,25D$_3$ and 1,4β,25D$_3$ ligands (Figure 1B) and the results gained from luciferase reporter assays in transfected human osteosarcoma cells indicated that both isomers are less active than 1,25D$_3$ [16,17]. Interestingly, significant differences in CYP24A1-induced 1,4,25D$_3$ metabolism are observed between the two isomers, and only the 4α isomer has been shown to be glucuronidated by certain hepatic UGT(s) [17,18]. In addition, the 4β,25D$_3$ has been shown to have a greater metabolic stability and resistance to CYP24A1 than 4α,25D$_3$ [19].

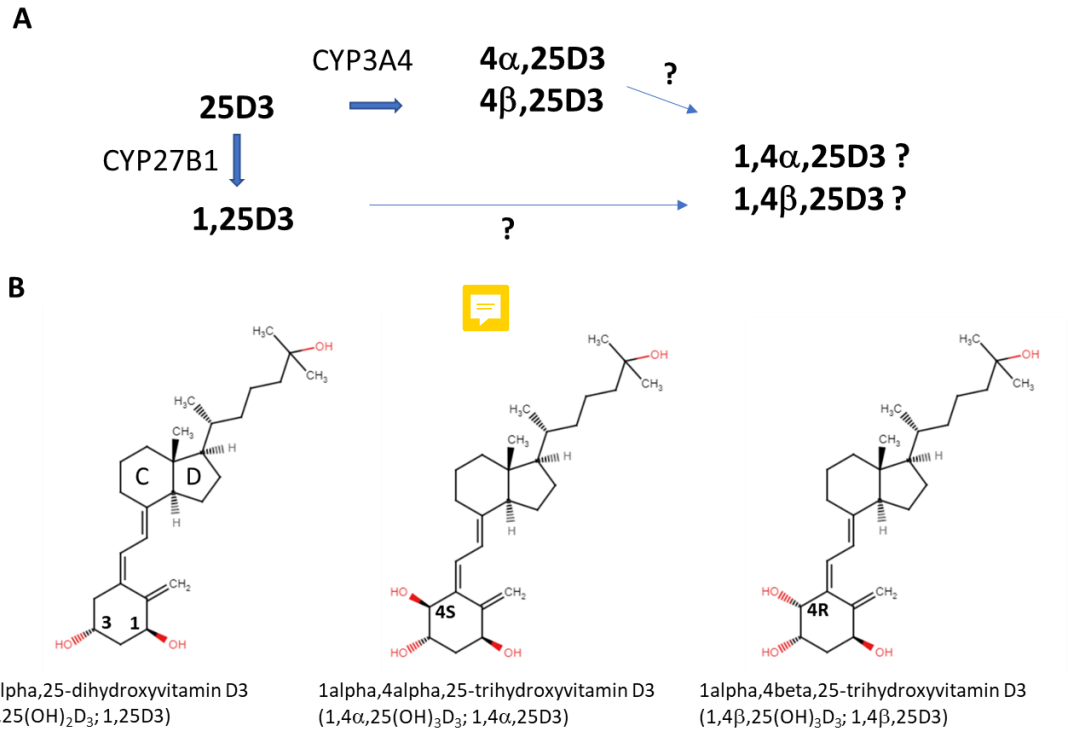

Figure 1. (A) Pathway of the production of 4-hydroxy metabolites of D3. **(B)** Chemical structures of the ligands.

To further unveil the structure-activity relationships of the 4-hydroxylated-1,25D$_3$-VDR complexes, we describe a detailed synthetic route to the synthesis of 1,4α,25D$_3$, and 1,4β,25D$_3$, as well as some of the biological properties and the crystal structures of their complexes with the VDR ligand binding domain (LBD).

2. Materials and Methods

2.1. Synthesis. General Information

All manipulations were performed under an argon atmosphere unless otherwise mentioned. All solvents and reagents were purified when necessary, using standard procedure. Column chromatography was performed on silica gel 60N (Kanto Chemical Co., Inc., 100-210 μm), flush column chromatography was performed on silica gel 60 (Merck, 0.040-0.063 mm), and preparative thin-layer chromatography was performed on silica gel

60 F_{254} (Merck, 0.5 mm). NMR spectra were measured on JEOL AL-400 (^{1}H at 400 MHz) and ECP-600 (^{13}C at 150 MHz) nuclear magnetic resonance spectrometers. Specific optical rotations were measured on JASCO DIP-370 digital polarimeter.

2.2. Biochemistry

The cDNA encoding His-tagged zVDR LBD (156-453) was cloned into pET28b. The recombinant proteins were produced in Escherichia coli BL21 DE3, grown ON at 18 °C after induction with 1 mM IPTG at an OD600 of ~0.7. Soluble proteins were purified on Ni Hitrap FFcrude column (Cytiva), followed by His tag removal by thrombin cleavage and by size exclusion chromatography on HiLoad Superdex 75 column (Cytiva) equilibrated in Tris 20 mM pH7, NaCl 200 mM, TCEP 1 mM. The proteins were concentrated to 3-7 mg/mL with an Amicon Ultra 10 kDa MWCO.

2.3. Thermal Unfolding, Differential Scanning Fluorimetry (nanoDSF)

Fluorescence based thermal experiments were performed using Prometheus NT.48 (NanoTemper Technologies, Germany) with capillaries containing 10 µL zVDR LBD at 3.2 mg/mL in absence and presence of 2 equivalent ligands and/or 4 equivalents of NCOA1 NR2 peptide (RHKILHRLLQEGSPS). The temperature was increased by a rate of 1 °C/min from 20 to 95 °C and the fluorescence at emission wavelengths of 330 nm and 350 nm was measured. NanoTemper PR.Stability Analysis v1.0.2 was used to fit the data and to determine the melting temperatures Tm. Triplicates of each sample were made.

2.4. Fluorescence Polarization

Steady-state fluorescence polarization measurements were performed with a PHERAstar Plus (BMG Labtech) spectrofluorometer. Titrations were carried out by adding increasing zVDR LBD concentrations to 10 nM Fluorescein-NCOA1 NR2 peptide (FL-LTARHKILHRLLQEGSPSD) in 50 mM Hepes pH8.0, 50 mM NaCl, 2% glycerol, 1 mM TCEP, 0.05% Tween-20. Binding affinity of the FL-peptide to zVDR LBD was quantified in response to 1,25D3, 1,4α,25D3 or 1,4β,25D3. The excitation wavelength was 488 nm and the emitted light was monitored through high-pass filters (520nm). The dissociation constant (Kd) was calculated using GraphPad Prism 10 by fitting agonist vs response equation. All experiments were performed at 25°C and results are representative of three distinct experiments.

2.5. Crystallization and Structure Determination

The concentrated protein at 5mg/mL was incubated with a 2-fold excess of ligand and a 3-fold excess of the coactivator NCOA2 (KHKILHRLLQDSS) peptide. The crystallization experiments were carried out by hanging drop vapor diffusion at 290 K by mixing equal volume (1µl) of protein-ligand complex and of reservoir solution (0.1 M MES pH 6.0,2.5 M NaOAc). The crystals of the complex were transferred to artificial mother liquor containing 0.1 M MES pH 6.0,3 M NaOAc and flash cooled in liquid nitrogen. Data from crystals of zVDR-1,4α,25D_3 and of zVDR-1,4β,25D_3 were collected on the Proxima2 beamline at Soleil synchrotron. The crystallographic raw data were processed with XDS [20] and scaled with AIMLESS [21]. The structures were solved and refined using Phenix [22] and iterative model building using COOT [23]. Crystallographic refinement statistics are presented in Supplementary Table 1.

2.6. Cells

IEC-18 rat intestinal epithelial cells (American Type Culture Collection, Rockville, USA) were grown in Dulbecco's modified Eagle's medium (DMEM) 4.5 g/l glucose supplemented with 5 % fetal calf serum (FCS), 1 mM Sodium Pyruvate, 0.1 UI/mL insulin and 40 µg/mL gentamicin. Cells at 80 % confluency were grown in medium supplemented with 5% charcoal-treated FCS for 24 h and treated as indicated.

2.7. Mice

A cohort of C57BL6J mice aged between 8 and 12 weeks were daily treated per os for 4 days with 1 μg/kg/day of 1,25D3, 1,4α,25D3 or 1,4β,25D3 in 100 μL oil [24]. On day 4, blood and kidneys were harvested for analysis. A cohort of mice treated with 100 μL oil is used as a control.

2.8. Functional Assay

Total RNA from IEC-18 cells and kidney were isolated using TRI Reagent (Molecular Research Center, Inc), according to the manufacturer's protocols. RNA was quantified by spectrophotometry (Nanodrop, Thermo Fisher, Illkirch, France), and cDNA prepared using 2 μg of total RNA, random hexamers, and SuperScript IV reverse transcriptase (Thermo Fisher, Illkirch, France), following the manufacturer's instructions. Quantitative PCR (Light Cycler 480-II) was performed using the Light Cycler 480 SYBR Green I Master X2 Kit (Roche Diagnostics, Meylan, France), according to the supplier's protocol. The data were analyzed using the standard curve method, following the manufacturer's protocol (Lightcycler 480 II, Roche Diagnostics, Meylan, France), and the 18S housekeeping gene as an internal control. The sets of primers used were the following: Cyp24a1 (rat), 5′-TCCATGAGGCTTACCCCAAG-3′ (sense) and 5′-GCGTATTCACCCAGAACCGT-3′ (antisense); S100g (rat), 5′-GACAGCAAGCAGCACAGAAAA-3′ (sense) and 5′-TGGACAGCTGGTTTGGATCG-3′ (antisense); Trpv6 (rat), 5′-GAGCACAGGTTGTGGCTACT-3′ (sense) and 5′-CCAAGACCATACTCTCGCCC-3′ (antisense); 18S (rat), 5′-AGCTCACTGGCATGGCCTTC-3′ (sense) and 5′-CGCCTGCTTCACCACCTTC-3′ (antisense); Cyp24a1 (mouse), 5′-GGCGGAAGATGTGAGGAATA-3′ (sense) and 5′-GCCCAGCACTTGGGTATTTA-3′ (antisense); Cyp27b1 (mouse), 5′-CGTCCAGAGCGCTGTAGTT-3′ (sense) and 5′-TCTTCACCATCCGCCGTTAG-3′ (antisense); Trpv5 (mouse), 5′-TGGTGGGTCAGAGACCAAG-3′ (sense) and 5′-CAGTGGAGACTCCCAAATACTTTT-3′ (antisense); 18s (mouse), 5′-AGCTCACTGGCATGGCCTTC-3′ (sense) and 5′-CGCCTGCTTCACCACCTTC-3′ (antisense)

2.9. Serum Calcium Levels

Mouse blood was collected in Microvette® 500 lithium heparin (SARSTEDT), and centrifuged at 400 g for 10 minutes at 4°C. The supernatant corresponding to the serum was retained. Serum calcium levels were determined using a colorimetric assay (MAK022, Sigma Aldrich), in accordance with the supplier's instructions.

3. Results and Discussion

3.1. Synthesis

Compounds 1,4 ,25D3 (**1a)** and 1,4 ,25D3 (**1b)** were synthesized as follows: the A-ring precursors enyne **2a** and **2b** were synthesized from methyl a-D-glucopyranoside by our reported procedures [17], and stereochemistry at the C4-position (4*R*) of the major product **2b** was determined by the modified Mosher's method [16,25].

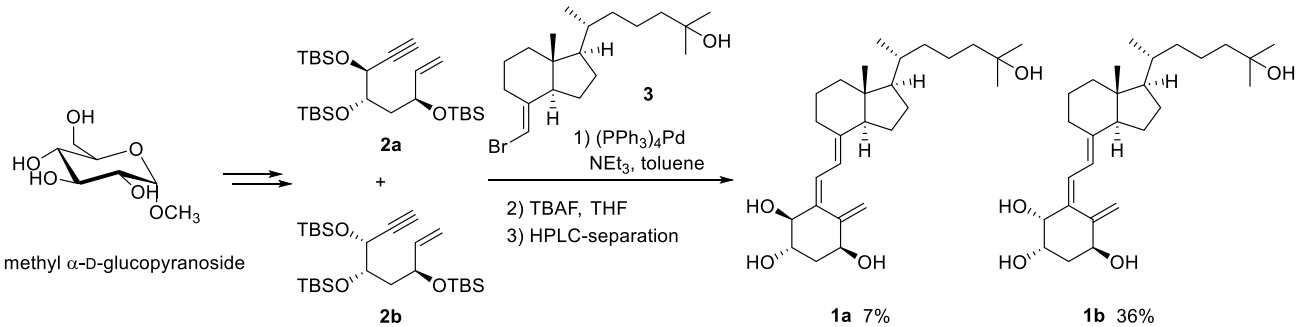

Scheme 1. Synthesis of 1α,4α,25-trihydroxyvitamin D3 (**1a**) and 1α,4β,25-trihydroxyvitamin D3 (**1b**).

To a solution of the enyne mixture (without separation of **2a** and **2b**, 95 mg, 190 mol, **2a**/**2b** = 1/3) and bromoolefin **3** (81 mg, 230 mol) in toluene (1.9 mL) were added triethylamine (1.9 mL) and Pd(PPh3)$_4$ (21 mg, 190 mol) at room temperature, and the reaction mixture was stirred at 80°C overnight. After cooling to room temperature, the mixture was concentrated in vacuo. The residue was purified by flush column chromatography on silica gel (hexane/EtOAc = 20/1) to give coupling products of silyl-protected **1a** and **1b** as an inseparable mixture (63 mg, 43% from enynes) as a pale yellow oil. This was used for the next reaction without further purification.

To a solution of the mixture of silyl-protected **1a** and **1b** (30 mg, 39 mol) in THF (0.8 mL) was added TBAF (0.4 mL, 1.0 M solution in THF, 400 mol) at 0°C, and the reaction mixture was stirred at room temperature for 3 h, and then at 80°C for 5 h. After cooling, the reaction was quenched by water at 0°C. The mixture was extracted with EtOAc, and the organic layer was washed with brine, dried over Na_2SO_4, filtered and concentrated. The residue was purified by preparative silica gel TLC plate (hexane/EtOAc = 2/1) to give the mixture of **1a** and **1b** (17 mg, quant) as a pale-yellow oil. The mixture was re-purified and separated by reversed-phase HPLC (YMC-Pack ODS column, 20 x 250 mm, CH_3OH/H_2O = 9/1) to give **1a** (1.2 mg,) and **1b** (6.4 mg) each as a colorless oil [17].

3.2. Biological Assays

Nano differential scanning fluorimetry analysis confirmed the binding of the 1,4 ,25(OH)$_3$D$_3$ and 1,4 ,25(OH)$_3$D$_3$ ligands to the zebrafish (z)VDR LBD that has been shown to similarly bind ligands as the human VDR [26]. The two 4-hydroxylated ligands increase the stabilization of the zVDR LBD, that is further increased in the presence of a NCOA1 coactivator peptide that encompasses one nuclear receptor LXXLL interacting motif (Figure 2A). However, the stabilization of the complexes is weaker compared to the effect of 1,25D$_3$ in this assay. The interaction with the NCOA1 coactivator peptide to the LBD of zVDR was next quantified by fluorescence polarization in the presence of saturating ligand concentration of 1,25D3, 1,4 ,25D$_3$ or 1,4 ,25D$_3$ (Figure 2B). Whereas the zVDR LBD in its apo form do not bind the NCOA1 peptide (data not shown), NCOA1 peptide binds to zVDR LBD with a similar affinity in the presence of the tested ligands (Kd = 0.54 µM, 0.50 µM and 0.48 µM for 1,25D$_3$, 1,4 ,25D$_3$ and 1,4 ,25D$_3$ complexes, respectively).

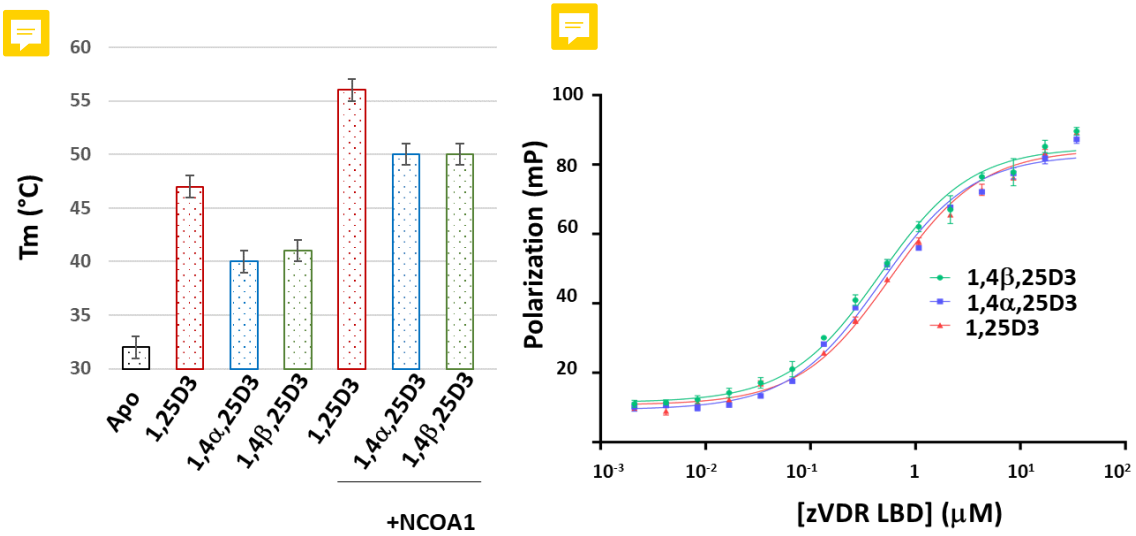

Figure 2. Effect of ligands on VDR stability and interaction with NCOA1. (**A**) Thermal stability of the purified zVDR LBD alone and upon binding to the ligands in absence or presence of the NCOA1 NR2 coactivator peptide. (**B**) 4hydroxy-1,25D$_3$-bound VDR LBD efficiently recruits NCOA1 coactivator peptide. Titration of the fluorescein- NCOA1 peptide with zVDR LBD in complex with 1,25D$_3$ (in red), 1,4α,25D$_3$ (in blue) or 1,4β,25D$_3$ (in green).

The effects of these 4(OH) ligands on VDR activities were previously studied using reporter gene assays [16,17]. To determine their potency to induce endogenous VDR target genes in intestinal cells, a key vitamin D target tissue, we evaluate the expression of transcript levels of several VDR target genes (*Cyp24a1*, *Trpv6* and *S100g*,) in rat intestinal epithelial (IEC-18) cells treated for 24 h with vehicle or 100 nM of 1,25D$_3$, 1,4 ,25D$_3$ and 1,4 ,25D$_3$ by RT-qPCR. The transcript levels of these VDR target genes were at least 2-fold induced in the presence of the compound tested compared to vehicle treated cells (Figure 3). Consequently, the 4-hydroxylated compounds are potent VDR agonist ligands with a potency comparable to that of 1,25D$_3$. Note that *Cyp24a1* transcripts were higher in 1,4 ,25D$_3$-treated cells than in 1,25D$_3$- and 1,4 ,25D$_3$ treated cells, indicating that 1,4 ,25D$_3$ is more potent. Thus, in contrast to the previous study using reporter assays in VDR transfected cells, the two metabolites enhance endogenous VDR activities in IEC-18 cells.

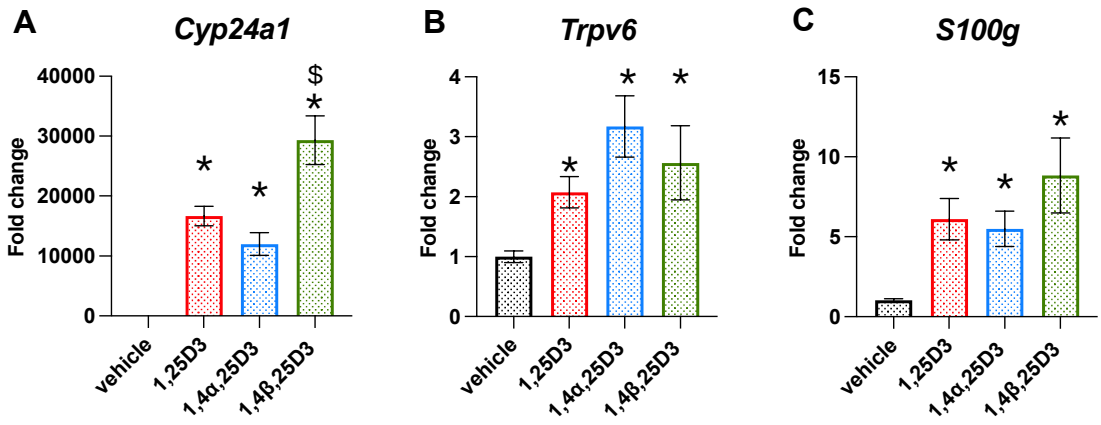

Figure 3. Relative transcript levels of VDR target genes in IEC-18 cells treated for 24 h with vehicle or 100 nM of the indicated ligands, determined by RT-qPCR (n = 4 biological replicates). *: p<0,05 vs Veh and $: p<0,05 vs 1,25D$_3$. One-way ANOVA followed by Tukey's test.

The results in IEC18 cells prompt us to investigate the *in vivo* activities of 1,4α,25D$_3$ and 1,4β,25D$_3$. We determined the effects of 1,4α,25D$_3$ and 1,4β,25D$_3$ administration on the expression of the VDR target genes *Cyp24a1* and *Cyp27b1*, two genes encoding proteins involved in the metabolic pathway of vitamin D and known to be upregulated and downregulated by 1,25D$_3$, respectively. After treatment with the 4-hydroxylated metabolites, Cyp24a1 transcript levels are induced whereas the expression of Cyp27b1 decreased. The expression of Trpv5, a VDR target gene encoding for a channel involved in kidney calcium reabsorption, is induced by 1,4α,25D$_3$ or 1,4β,25D$_3$ with a similar potency than 1,25D$_3$. Then, we determined pro-calcemic activities of the 4-hydroxylated metabolites. In accordance with previous results, mice treated with 1 µg/kg/day 1,25D$_3$ for 4 days are hypercalcemic [26]. Interestingly, serum calcium levels after 1,4α,25D$_3$ or 1,4β,25D$_3$ intoxication are similar to those in 1,25D$_3$ treated mice. All together, these results indicate that 1,4α,25D$_3$ or 1,4β,25D$_3$ have comparable *in vivo* activities to thoseof 1,25D$_3$.

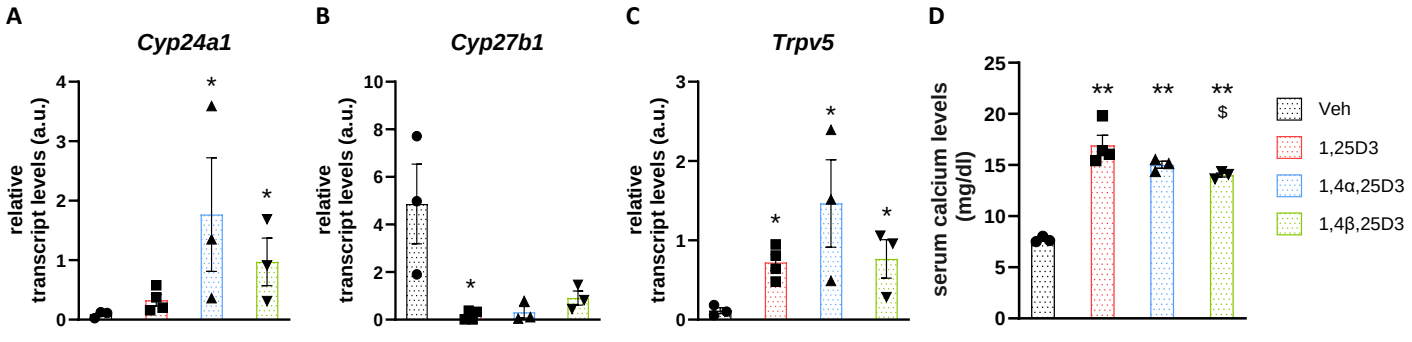

Figure 4. Relative renal transcript levels of the VDR target genes Cyp24a1 (A), Cyp27b1 (B) and Trpv5 (C), and serum calcium levels (D) in WT mice daily treated for 4 days with vehicle (Veh) or 1 µg/kg/day of the indicated ligands determined by RT-qPCR and colorimetric test, respectively (n=3-4; Each point represents an animal). **: p<0,001 and *: p<0,05 vs Veh; $: p<0,05 vs 1,25D3. One-way ANOVA followed by Tukey's test.

3.3. Ligand Binding Mode to VDR

To decipher the ligand binding mode of the two 4-hydroxy metabolites to VDR, we solved the crystal structures of their complexes with the zVDR LBD in presence of a NCOA2 coactivator peptide. The structures of zVDR LBD bound to 1,4 ,25D3 and to 1,4 ,25D3 were determined at a resolution of 1.95 and 1.8 Å, respectively. The crystallographic data are summarized in Supplementary Table 1. After refinement of the protein alone, the map showed an unambiguous electron density where to fit the ligands (Supplementary Figure 1). The complexes formed by the zVDR LBD bound to the two 4-OH compounds adopt the canonical active conformation as described in all previously reported agonist-bound VDR. When compared to the structure of zVDR LBD-1,25D3 complex, the atomic coordinates of zVDR LBD bound to 1,4 ,25D3 and 1,4 ,25D3 show very small root-mean-square deviation of 0.3 Å over 235 Cα atoms, reflecting the high structural homology.

The addition of an additional hydroxyl group on C4 does not modify the A-ring conformation of the ligand and the seco-B, C/D-rings and aliphatic side chain have similar conformation to those of 1,25D3 (Figure 5A). The distances between the C1-OH and C25-OH are 13.12Å, 13.11Å and 12.95Å, and between the C3-OH and C25-OH are 15.36 Å, 15.38 Å and 15.28 Å, for 1,25D3, 1,4 ,25D3 and 1,4 ,25D3, respectively. The interactions between the secoB, C, D-rings and side chain are similar to those formed by the 1,25D3, as well as the hydrogen bonds formed with the 1-OH, 3-OH and 25-OH (Figure 5B-C). Differences are observed around the 4-OH group; the 4-OH group of the 4 metabolite forms hydrogen bonds with Ser306 and Cys316, whereas its diastereomer 4 acts through hydrogen bonding only with Cys316 but ~~form~~ stronger van der Waals interactions with Phe182 and Leu261 (Figure 5D-E). To adapt the additional hydroxyl group, few side chains amino acids residues are slightly shifted, notably Tyr179, Phe182 and Cys316 by 0.4-0.6 Å.

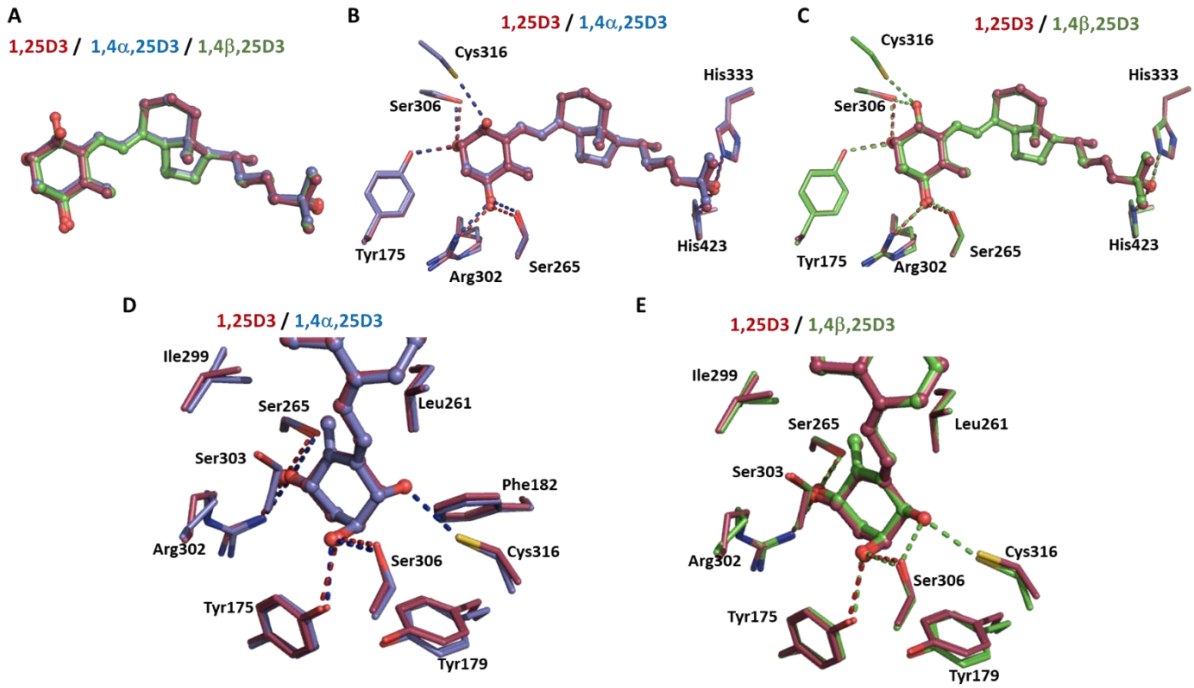

Figure 5. Ligand binding mode. (A) Conformation of the bound ligands in the VDR LBD complexes. The ligands, 1,25D$_3$ (red), 1,4α,25D$_3$ (blue) and 1,4β,25D$_3$ (green) are shown in stick representation after superimposed VDR complexes. **(B)** Hydrogen bonds formed by the hydroxyl groups of 1,4α,25D$_3$ (blue) and 1,25D$_3$ (red) in the LBP of the zVDR. **(C)** Hydrogen bonds formed by the hydroxyl groups of 1,4β,25D$_3$ (green) and 1,25D$_3$ (red) in the LBP of the zVDR. **(D-E)** Close up view of the superimposed ligands around the A-ring of the ligands: 1,4α,25D$_3$ (blue), 1,4β,25D$_3$ (green), 1,25D$_3$ (red). Residues side-chains closer than 4.0 Å contacting the ligands are shown. The hydrogen bonds formed by the ligands are shown as dashed lines.

These structural data agree well with the induced biological activity of the two compounds that are similar to the natural hormone. Other natural metabolites have been shown to retain significant biological activity compared to the natural hormone, notably the 1,25(OH)$_2$-3epi-D$_3$ that compensates the loss of interaction of the 3-OH group with hSer278 by a water-mediated hydrogen bond[23] or the 20S-hydroxy-D3[24]. In addition, some A-ring modified analogs at C2 have been shown to have a better affinity for VDR and to be more resistant to CYP24A1 catabolism[25].

4. Conclusions

We described the synthesis of the 1α,4α,25D$_3$, and 1α,4β,25D$_3$ ligands. The crystal structures of zVDR LBD in complex with the two epimers provide a mechanistic insight for the specific recognition of the 4-hydroxy metabolites of 1,25D$_3$. Indeed, the crystal structures reveal that the 4-hydroxylated metabolites maintain the anchoring H-bonds of 1,25D$_3$ and form additional interactions. In IEC-18 cells, the two compounds are potent VDR agonist ligands with a similar potency to 1,25D$_3$. In addition, they regulate the expression of renal VDR target genes, and increase serum calcium levels, demonstrating that these 4-hydroxylate metabolites enhance VDR activities in vivo. Therefore, we conclude that the C4-hydroxylation pathway produces active metabolites with similar biochemical and biological properties to those of the 1,25D$_3$. However, whereas the 4,25D$_3$ are endogenous metabolites, the occurrence of C4-hydroxylation on 1,25D$_3$ or C1-hydroxylation of 4,25D$_3$ remain to be demonstrated. The high and differential metabolic stability together with the significant biologic activity make these synthetic 4-hydroxy analogs interesting ligands for clinical applications.

Acknowledgments: We thank A. McEwen for help in X-ray data collection, and the staff of PX2 beam line of SOLEIL synchrotron for assistance during X-ray data collection. The research was also supported by French Infrastructure for Integrated Structural Biology (FRISBI) [ANR-10-INBS-05]; Instruct-ERIC; Agence Nationale de la Recherche under the program Investissements d'Avenir [ANR-10-LABX-0030-INRT, ANR-10-IDEX-0002-02].

Supporting Information: The SI contains structural data.

Accession Codes: The atomic coordinates and structure factors have been deposited with accession codes xx. Authors will release the atomic coordinates upon article publication.

References

1. Fleet, J. C. The role of vitamin D in the endocrinology controlling calcium homeostasis. *Mol. Cell Endocrinol.* **2017**, *453*, 36-45.
2. Goltzman, D. Functions of vitamin D in bone. *Histochem. Cell Biol*. **2018**, *149*, 305-312.
3. Vanherwegen, A.S.; Gysemans, C.; Mathieu, C. Regulation of Immune Function by Vitamin D and Its Use in Diseases of Immunity. *Endocrinology and Metabolism Clinics of North America* **2017**, *46*, 1061-1094.
4. Christakos, S.; Dhawan, P.; Verstuyf, A.; Verlinden, L.; Carmeliet, G. Vitamin D: Metabolism, molecular mechanism of action, and pleiotropic effects. *Physiol. Rev*. **2016**, *96*, 365-408.
5. Rochel, N. Vitamin D and Its Receptor from a Structural Perspective. *Nutrients*. **2022**, *14*, 2847.
6. Bouillon, R; Bikle, D. Vitamin D Metabolism Revised: Fall of Dogmas. *J Bone Miner Res.* **2019**, *34*, 1985-1992.
7. Sakaki, T.; Kagawa, N.; Yamamoto, K.; Inouye, K. Metabolism of vitamin D3 by cytochromes P450. *Front Biosci.* **2005,** *10*, 119-134.
8. Jenkinson, C. The vitamin D metabolome: An update on analysis and function. *Cell Biochem Funct.* **2019**, *37*, 408-423.
9. Tuckey, R.C.; Cheng, C.Y.S.; Slominski, A.T. The serum vitamin D metabolome: What we know and what is still to discover. *J Steroid Biochem Mol Biol.* **2019**, *186*, 4-21.
10. Reddy, G.S.; Rao, D.S.; Siu-Caldera, M.L.; Astecker, N.; Weiskopf, A.; Vouros, P.; Sasso, G.J.; Manchand, P.S.; Uskokovic, M.R. 1alpha,25-dihydroxy-16-ene-23-yne-vitamin D3 and 1alpha,25-dihydroxy-16-ene-23-yne-20-epi-vitamin D3: analogs of 1alpha,25-dihydroxyvitamin D3 that resist metabolism through the C-24 oxidation pathway are metabolized through the C-3 epimerization pathway. *Arch Biochem Biophys*. **2000**, *383*, 197-205.
11. Rao, D.S.; Dayal, R.; Siu-Caldera, M.L.; Horst, R.L.; Uskokovic, M.R.; Tserng, K.Y.; Reddy, G.S. Isolation and identification of 4,25-dihydroxyvitamin D2: a novel A-ring hydroxylated metabolite of vitamin D2. *J Steroid Biochem Mol Biol*. **1999**, *71*, 63-70.
12. Wang, Z.; Lin, Y.S.; Zheng, X.E.; Senn, T.; Hashizume, T.; Scian, M.; Dickmann, L.J.; Nelson, S.D.; Baillie, T.A.; Hebert, M.F.; Blough, D.; Davis, C.L.; Thummel, K.E. An inducible cytochrome P450 3A4-dependent vitamin D catabolic pathway. *Mol Pharmacol*. **2012,** *81*, 498-509.
13. Wang, Z.; Lin, Y.S.; Dickmann, L.J.; Poulton, E.J.; Eaton, D.L.; Lampe, J.W.; Shen, D.D.; Davis, C.L.; Shuhart, M.C.; Thummel, K.E. Enhancement of hepatic 4-hydroxylation of 25-hydroxyvitamin D3 through CYP3A4 induction in vitro and in vivo: implications for drug-induced osteomalacia. *J Bone Miner Res.* **2013**, *28*, 1101-1116.
14. Roizen, J.D.; Li, D.; O'Lear, L.; Javaid, M.K.; Shaw, N.J.; Ebeling, P.R.; Nguyen, H.H.; Rodda, C.P.; Thummel, K.E.; Thacher, T.D.; Hakonarson, H.; Levine, M.A. CYP3A4 mutation causes vitamin D-dependent rickets type 3. *J Clin Invest*. **2018,** *128*, 1913-1918.
15. Horst, R.L.; Wovkulich, P.M.; Baggiolini, E.G.; Uskoković, M.R.; Engstrom, G.W.; Napoli, J.L. (23S)-1,23,25-Trihydroxyvitamin D3: its biologic activity and role in 1 alpha,25-dihydroxyvitamin D3 26,23-lactone biosynthesis. *Biochemistry*. **1984**, *23*, 3973-3979.
16. Sawada, D.; Tsukuda, Y.; Saito, H.; Takagi, K.; Horie, K.; Ochiai, E.; Takenouchi, K.; Kittaka, A. Synthesis and biological evaluation of 4-substituted vitamin d and 14-epi-previtamin d analogs. *Chem Pharm Bull (Tokyo)*. **2009**, *57*, 1431-1433.
17. Sawada, D.; Tsukuda, Y.; Yasuda, K.; Sakaki, T.; Saito, H.; Takagi, K.; Takenouchi, K.; Chen, T.C.; Reddy, G.S.; Kittaka, A. Synthesis and biological activities of 1α,4α,25- and 1α,4β,25-trihydroxyvitamin D(3) and their metabolism by human CYP24A1 and UDP-glucuronosyltransferase. *Chem Pharm Bull (Tokyo)*. **2012**, *60*, 1343-1346.
18. Takano, M.; Sawada, D.; Yasuda, K.; Nishikawa, M.; Takeuchi, A.; Takagi, K.; Horie, K.; Reddy, G.S.; Chen, T.C.; Sakaki, T.; Kittaka, A. Synthesis and metabolic studies of 1α,2α,25-, 1α,4α,25- and 1α,4β,25-trihydroxyvitamin D3. *J Steroid Biochem Mol Biol.* **2015,** *148*, 34-37.
19. Mizumoto, Y.; Sakamoto, R.; Iijima, K.; Nakaya, N.; Odagi, M.; Tera, M.; Hirokawa, T.; Sakaki, T.; Yasuda, K.; Nagasawa, K. Differential Metabolic Stability of 4α,25- and 4β,25-Dihydroxyvitamin D3 and Identification of Their Metabolites. *Biomolecules* **2023**, *13*, 1036.
20. Kabsch, W. Software XDS for image rotation, recognition and crystal symmetry assignment. *Acta Crystallogr., Sect. D: Biol. Crystallogr.* **2010**, *66*, 125−132.
21. Evans, P. Scaling and assessment of data quality. *Acta Crystallogr. Sect. D: Biol. Crystallogr.* **2006**, *62*, 72−82.
22. Adams, P.D.; Afonine, P.V.; Bunkoczi, G.; Chen, V.B.; Davis, I.W.; Echols, N.; Headd, J.J.; Hung, L.W.; Kapral, G.J.; Grosse-Kunstleve, R.W.; et al. PHENIX: a comprehensive Python-based system for macromolecular structure solution. *Acta Crystallogr D Biol Crystallogr*. **2010**, *66*, 213-221.
23. Emsley, P.; Cowtan, K. Coot: model-building tools for molecular graphics. *Acta Crystallogr. Sect. D: Biol. Crystallogr.* **2004**, *60*, 2126−2132.

24. Rovito, D.; Belorusova, A.Y.; Chalhoub, S.; Rerra, A.I.; Guiot, E.; Molin, A.; Linglart, A.; Rochel, N.; Laverny, G.; Metzger, D. Cytosolic sequestration of the vitamin D receptor as a therapeutic option for vitamin D-induced hypercalcemia. *Nat Commun*. **2020**, 11, 6249.
25. Ohtani, I.; Kusumi, T.; Kashman, Y.; Kakisawa, H. High-field FT NMR application of Mosher's method. The absolute configurations of marine terpenoids. *J. Am. Chem. Soc*. **1991**, *113*, 4092-4096.
26. Ciesielski, F.; Rochel, N.; Moras, D. Adaptability of the Vitamin D nuclear receptor to the synthetic ligand Gemini: remodelling the LBP with one side chain rotation. *J Steroid Biochem Mol Biol*. **2007**, *103*, 235-42.
27. Molnár, F.; Sigüeiro, R.; Sato, Y.; Araujo, C.; Schuster, I.; Antony, P.; Peluso, J.; Muller, C.; Mouriño, A.; Moras, D.; Rochel, N. 1α,25(OH)2-3-epi-vitamin D3, a natural physiological metabolite of vitamin D3: its synthesis, biological activity and crystal structure with its receptor. *PLoS One*. **2011**, *6*, e18124.
28. Lin, Z.; Marepally, S.R.; Goh, E.S.Y.; Cheng, C.Y.S.; Janjetovic, Z.; Kim, T.K.; Miller, D.D.; Postlethwaite, A.E.; Slominski, A.T.; Tuckey, R.C.; Peluso-Iltis, C.; Rochel, N.; Li, W. Investigation of 20S-hydroxyvitamin D3 analogs and their 1α-OH derivatives as potent vitamin D receptor agonists with anti-inflammatory activities. *Sci Rep*. **2018**, *8*, 1478.
29. Takano, M.; Ohya, S.; Yasuda, K.; Nishikawa, M.; Takeuchi, A.; Sawada, D.; Sakaki, T.; Kittaka, A. Synthesis and biological activity of 1α,2α,25-trihydroxyvitamin D3: active metabolite of 2α-(3-hydroxypropoxy)-1α,25-dihydroxyvitamin D3 by human CYP3A4. *Chem Pharm Bull (Tokyo)*. **2014**, *62*, 182-184.

Disclaimer/Publisher's Note: The statements, opinions and data contained in all publications are solely those of the individual author(s) and contributor(s) and not of MDPI and/or the editor(s). MDPI and/or the editor(s) disclaim responsibility for any injury to people or property resulting from any ideas, methods, instructions or products referred to in the content.